Nanoscale

REVIEW

View Article Online
View Journal | View Issue

Cite this: *Nanoscale*, 2023, **15**, 16874

Enhancement of MXene optical properties towards medical applications *via* metal oxide incorporation

Karolinekersin Enoch,[a] Aravindkumar Sundaram,[a] Stephen Selvamani Ponraj,[a] Sathya Palaniyappan,[a] Sahaya Dennis Babu George[b] and Rajesh Kumar Manavalan *[c]

Received 30th May 2023,
Accepted 2nd October 2023

DOI: 10.1039/d3nr02527f

rsc.li/nanoscale

MXenes have garnered research attention in the field of biomedical applications due to their unique properties, such as a large surface area, low toxicity, biocompatibility, and stability. Their optical behavior makes them versatile for a wide range of biomedical applications, from diagnostics to therapeutics. Nonetheless, MXenes have some minor limitations, including issues with restacking, susceptibility to oxidation, and a non-semiconducting nature. These limitations have prompted researchers to explore the incorporation of metal oxides into MXene structures. Metal oxides possess advantageous properties such as a high surface area, biocompatibility, intriguing redox behavior, catalytic activity, semiconducting properties, and enhanced stability. Incorporating metal oxides into MXenes can significantly improve their conductivity, surface area, and mechanical strength. In this review, we emphasize the importance of incorporating metal oxides into MXenes for light-influenced biomedical applications. We also provide insights into various preparation methods for incorporating metal oxides into MXene structures. Furthermore, we discuss how the incorporation of metal oxides enhances the optical behavior of MXenes. Finally, we offer a glimpse into the future potential of metal oxide-incorporated MXenes for diverse biomedical applications.

1. Introduction

The use of nanomaterials in biomedical applications is becoming increasingly crucial, offering significant support to the healthcare system and advancements in diagnostics and therapeutics. Many nanomaterials are used in biomedical applications like biosensors, drug delivery, bioimaging, and implants.[1,2] Different dimensional nanomaterials are employed in various biomedical applications since nanomaterials show many beneficial properties in different dimensions.[3] Two-dimensional nanomaterials have gained more attention in various biomedical applications due to their tunable surface area and electrical and optical properties.[4] In particular, graphene,[5] antimonene,[6] black phosphorus,[7] dichalcogenides,[8] and oxides[9] are widely used 2D nanomaterials in biomedical applications. Nevertheless, MXenes have gained immense attention in the 2D nanomaterials research[10] and have an idiosyncratic two-dimensional (2D) structure embedded with transition metal carbides, nitrides, and carbo-nitrides. These structures evolved in 2011 when Prof. Michel W. Barsoum and Prof. Yury Gogotsi from Drexel University, Philadelphia discovered the first-ever MXene–titanium-carbide layers by exfoliating 3D titanium aluminium carbide (Ti_3AlC_2) *via* the acid etching technique.[3] The geometrical structures of MXenes are symbolized as $M_{n+1}X_nT_x$, where M represents an early transition metal (such as Sc, Ti, Zr, Hf, V, Nb, Ta, Cr, Mo, Mn), X is C and N, T is an exterior windup unit especially hydroxyl, oxygen or fluorine groups, and n = 1, 2, or 3. Akin to graphene, MXenes are generally formed by exfoliating their 3D precursors, represented as a top–down approach.[4] The preparation and fabrication modalities of MXenes involve both the top and bottom scaling approaches, more specifically the top scaling methods are vastly applied relative to the bottom–up scaling methods that have seen rare utilization. The top–down scaling methods mainly comprise liquid-based chemical and mechanical exfoliation from the bulk crystal of the MAX phase. There are different types of MAX phases available like Ti_2AlC, Ti_2AlN, and V_2GeC, Ti_3SiC_2, Ti_3GeC_2, Ti_3AlC_2, Ti_3SnC_2, Ta_3AlC_2, Ti_4AlN_3, Ti_4SiC_3, Ti_4GeC_3, Ta_4AlC_3, Nb_4AlC_3, V_4AlC_3, and $Ti_4G_2C_3$.[11] The conversion of the MAX phase into MXene is generally performed *via* wet chemistry methods by means of etching the atomic (A) layers from their corresponding layered precursors (MAX phase) with the use of strong etchants

[a]*Centre for Advanced Materials, Aaivalayam – Dynamic Integrated Research Academy and Corporations (A-DIRAC), Coimbatore 641046, India*
[b]*Chettinad College of Engineering and Technology, Karur, 639114, India*
[c]*Institute of Natural Science and Mathematics, Ural Federal University, 620002 Yekaterinburg, Russia. E-mail: rajeshkumar_vgm@yahoo.com*

namely HF,[12] LiF,[13] NH_4HF_2,[14] and NH_4F.[15] In addition, non-HF etchants such as Lewis acids[16] and molten salts[17] (LiF, NaF, KF, NaOH) based electrochemical and hydrothermal methods have been introduced.[18]

As depicted in Fig. 1, the 3D precursors for MXenes are termed MAX phases, ternary carbides, or nitrides described with the general formula $M_{n+1}AX_n$, in which A stands for an A group element (mostly leading group IIIA or IVA). The A layers in MXenes are more active than the M–X layers. Because M–X bonds are much stronger than M–A bonds, A layers can be selectively etched using a strong acid (*i.e.*, hydrofluoric acid, HF) to produce $M_{n+1}X_n$ layers further detached by sonication.[19] The exterior of MXenes is typically winded up with fluorine (–F), hydroxide (–OH), and oxygen (–O) groups by the etching process, which provides high surface energy.[3] Hence, the final geometrical symbol of MXenes is displayed as $M_{n+1}X_nT_x$, where T_x is the surface functional group.[6] In addition, MXenes have various properties that can be employed in their fundamental prospects, such as structural, chemical, optical,[20] electronic, and even biological.[10] Many experimental and theoretical studies[20] explored the stupendous potential of MXenes for various applications in optoelectronics, photonics, catalysis, and many other areas.[19,21] MXenes emerge as new 2D nanoplatforms for advanced optoelectronics to be explored in various biomedical applications like biosensing,[22] bioimaging,[23] and therapeutic applications.[24,25] The essential mechanical and electronic properties can be attained by tailoring the elemental composition and chemical functionalization.[26] The exclusive traits of MXenes involve a high surface area, high atomic numbers (some transition metals), the presence of hydrophilic functional groups, and paramagnetic behaviour. The functional groups on MXenes also contribute to their rigidness and flexibility, which is crucial in thin film formation as part of bio-electronic devices.[27]

Most importantly, the high surface area is beneficial for drug loading and delivery for theranostic applications in various synergistic diseases. Furthermore, hydrophilic functional groups are also crucial for drug loading and targeted drug delivery, as modification or functionalization increases biocompatibility for living cells/tissues.[28,29] MXenes, comprising high atomic number and paramagnetic transition metals, are more relevant for biomedical imaging because they show superior X-ray attenuation for computed tomography (CT) scans and can also be employed as magnetic resonance imaging (MRI) contrast agents.[29] Distinct types of MXenes could be prepared based on different approaches; therefore, the biocompatibility assessment of MXene-based biomaterials is essential for general biomedical applications.[30] Metal oxides are widely employed in various biomedical applications in the diagnostic and therapeutic fields as they possess biocompatibility, a high surface area, good chemical and mechanical stability, and a unique structure.[31] Besides, the unique properties of metal oxides, such as enhanced electron transfer kinetics, strong adsorption capability, high sensitivity, and high optical absorption ability, make them more suitable for incorporation into MXenes. This enhances the optical properties for biomedical applications.[32,33] Metal oxides like TiO_2,[34] ZnO,[35] ZrO_2,[36] Fe_2O_3,[37] MnO_2,[38] MgO,[39] CeO_2,[40] and CuO[41] are broadly used in biomedical applications. In the part of the set, various metal oxide-based hybrid and composite formulations of MXenes were reported elsewhere for biomedical applications.[42–44] In recent years, the incorporation or coating of metal oxides over MXenes has gained prominence due to the substantial enhancement of their optical properties for various light-influenced medical applications.[45–47] This has sparked significant interest in understanding the underlying mechanisms of metal oxide incorporation into MXenes. However, to date, a comprehensive review of how the technology of metal oxide incorporation alone improves MXenes' optical properties and their applications in medicine has not been published.

This review emphasized the crucial part of tuning the optical properties of MXenes *via* incorporating metal oxides for different photo-influenced biomedical applications, as presented in Fig. 2. Also, the unique enhancement of the optical properties of MXenes using metal oxides resulting in advanced biomedical applications has been covered with recent tenets and trends. This review discussed the importance of incorporating metal oxides into MXenes to enhance their optical behavior. The different preparation methods for incorporating metal oxides into MXenes were covered, along with their advantages and disadvantages. This review emphasized the scope and challenges of metal oxides masked with MXenes for future research.

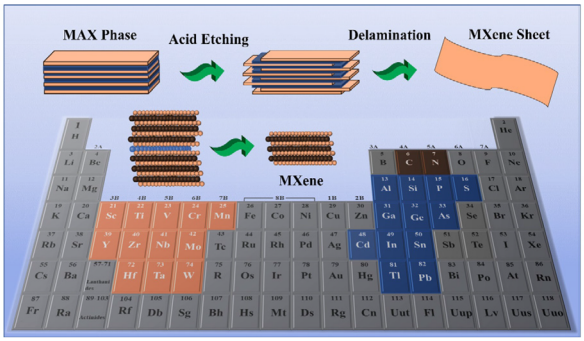

Fig. 1 Schematic representation of MAX phase elements in the periodic table and synthesis steps of MXenes from the MAX phase.

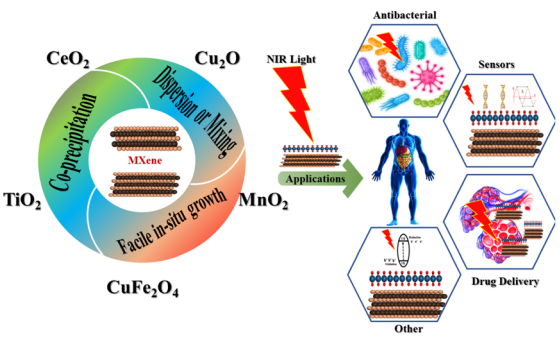

Fig. 2 Schematic overview of the review organization.

2. Complementing MXene with metal oxide composites

The optical properties of the MXene rely on the energy structures, the dispersion of linear and nonlinear dielectric function (ε), or the refractive index ($n = \sqrt{\varepsilon\mu}$).[48,49] MXenes have a linear absorption loss of ~1% nm^{-1},[50] a nonlinear absorption coefficient of about 10–21 m^2 V^{-2},[51] and a negative nonlinear refractive index of about 10–20 m^2 W^{-1}.[51] MXenes have exclusive characteristics, with enormous electrons gathered close to the Fermi level of MXene to serve as an electron reservoir, supplying decisive transfer of charge carriers. The beneficial properties of MXene include surface-modified functional groups that tune the bandgap of the obtained materials. These functional groups generate a negative charge on the surface of MXene, which electrostatically attracts the cations.[52] It also furnishes a platform to enhance interfacial contact between the semiconductor and MXenes, resulting in the transfer or separation of charge carriers in composites to enhance the optical properties.[53] Though MXene comprises many unique properties, it shows limitations like lack of semiconducting behaviour, restacking of MXene layers after exfoliation, easy oxidation, and low electrical conductivity.[54] It is also worth mentioning that metal oxides lack conductivity and have more significant band gaps. Hence, the heterostructures of MXenes incorporated with metal oxides exhibit favourable improvement in enhancing the optical properties to be employed in the photocatalytic performance for various biomedical applications. Different metal oxides, like SnO_2,[55] TiO_2,[56] and MnO_2,[57] have been incorporated into MXenes to enhance their optical properties. Several studies[58] suggested that incorporating $NiFe_2O_4$ into MXene heterostructures cogently assisted in averting the restacking of MXene flakes to increase the surface area of the heterostructure, and the surface area of MXene was found to be 19.26 and improved to 49.1812 m^2 g^{-1} after the incorporation of $NiFe_2O_4$.

3. Different methods to mask metal oxides in MXene composites

MXenes are typically synthesized by wet chemical acidic etching of MAX phases using robust etching solutions with fluoride ions (F^-) such as hydrofluoric acid (HF)[59] and ammonium bifluoride[60] and a mixture of hydrochloric acid and lithium fluoride. They can be prepared in single to few flakes or multiple stacks of MXene sheets. The morphology of MXenes can be tuned by adjusting the concentration of the etching solution, etching time, ultrasonication, and temperature. The literature also highlights exciting methods such as wet chemical reduction, self-oxidation, self-reduction, and pressure-less sintering for incorporating metal oxides into MXenes. Other techniques, including dry mixing/thermal pressing, solution blending, emulsion mixing, *in situ* polymerization, and lamination stacking, have also been utilized. Metal oxides are also connected with MXenes using simple chemical methods like blending and precipitation.

3.1 Co-precipitation method

Co-precipitation is a simple and fastest technique to prepare metal oxide-masked MXenes. This method has advantages like high yield, high product purity, and lack of necessity for organic solvents. As shown in Fig. 3, MXenes and metal oxides are dispersed in a suitable solvent at a particular temperature with a suitable reducing agent and the pH is maintained to form intermediate precipitates resulting from nucleation and growth.[61,62] The parameters like temperature, pressure, concentration, pH, stirring speed, and reaction time are of significant concern in controlling nanostructure size and shape distribution. First, the[63] MXenes are dispersed in a specified solvent, mostly in distilled water, followed by the addition of the precursor for metal oxide with either a suitable stabilizing agent or targeting moieties depending upon application usage. For instance, for anti-bacterial application, Ti_3C_2 is masked using cuprous oxide (Cu_2O).[63]

As depicted in Fig. 4, aminated MXenes reacted with cupric nitrate trihydrate as a precursor for synthesizing Cu_2O and polyvinylpyrrolidone (PVP), and hydrazine hydrate is used as stabilizing and reducing agents, respectively.[63] A similar and simple synthesis approach is attempted for preparing the Cu_2O/MXene composite with copper(II) sulfate, PVP, and N_2H_2 as the precursor, stabilizing, and reducing agents, respectively.[64] To support the co-precipitation synthesis route, various metal oxide-masked MXenes are synthesized, such as Ti_3C_2/Al_2O_3/Ag,[65] Ti_3C_2/SiO_2/Ag,[66] and Ti_3C_2/SiO_2/Pd,[66] Ti_3C_2F/$FeWO_4$,[67] TiO_2/Ti_3C_2/Cu_2O, and WO_3/MXenes.[45]

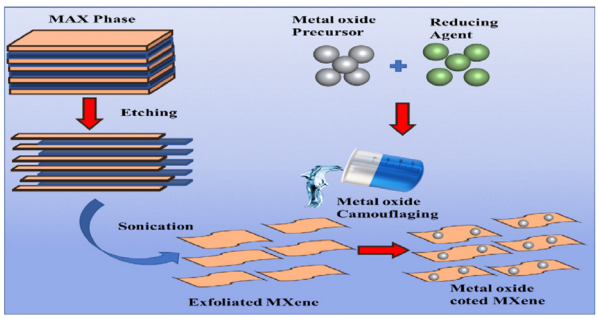

Fig. 3 Schematic illustration of MXene/metal oxide synthesis *via* the co-precipitation method.

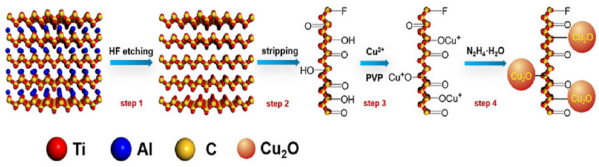

Fig. 4 Schematic illustration of the etching, striping and reduction process of Cu_2O/MXene synthesis *via* the co-precipitation method. (Reproduced with permission from ref. 64 Copyright, 2020 Elsevier.)

3.2 Dispersion or mixing

Another approach for preparing MXene/metal oxide nanocomposite is the dispersion of both MXene/metal oxide in a suitable solvent under ultrasonication, as depicted in Fig. 5. Ultrasonication mixing or mechanical stirring assists in properly distributing MXene/metal oxide to form a composite after removing the solvent and drying. In general, the parameters like ultrasonication power and frequency, temperature, and ultrasonication time play a crucial role in this method. Following a longer sonication time and less ultrasonication power is essential for proper dispersion.[68] As evidence, Fig. 6 shows the dispersion or mixing method of CuO-masked MXene preparation *via* the ultrasonication route for photocatalytic anti-bacterial applications.[46] The composites, $NiFe_2O_4$/MXene[58] and $CuFe_2O_4/Ti_3C_2$,[69] were also prepared by dispersion in an ultrasonicated water bath for an hour, followed by vacuum drying.

3.3 Facile *in situ* growth

Fig. 7 shows the facile *in situ* technique; redox reactions grow the metal oxide *in situ* over the MXene exterior. For example, Fig. 8 shows the *in situ* growth of iron-oxide on the surface of Ta_4C_3 MXene according to the redox reaction of MXene for photoactivated cancer theranostic applications. The exterior is stabilized or modified with soybean phospholipids for enhanced delivery of nanoparticles at the site of action. Akin to the abovementioned technique, manganese oxide is grown over Ti_3C_2[70] by a simple redox reaction for cancer therapeutics. Briefly, the $KMnO_4$ aqueous solution was mixed with Ti_3C_2 aqueous solution under magnetic stirring at room temperature, followed by centrifugation resulting in the composite nanosheet. The challenge is that many MXenes need to be fabricated from the MAX phase before mixing, and sometimes it requires retaining the stratified architecture to supply more cavities for metals or metal compounds to be deposited.

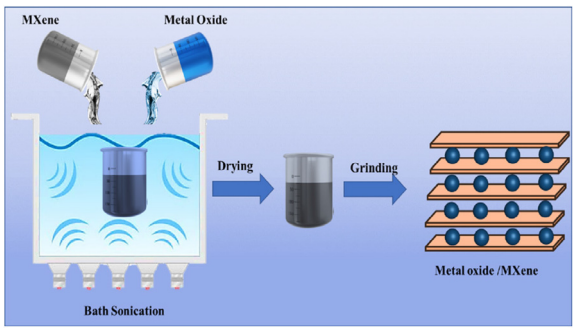

Fig. 5 Schematic representation of MXene/metal oxide synthesis *via* the dispersion or mixing method.

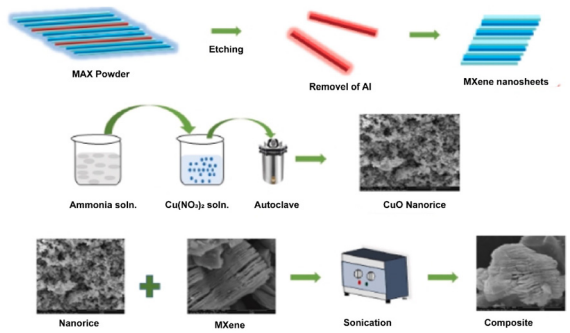

Fig. 6 Schematic illustration of CuO/MXene synthesis *via* the dispersion/mixing method. (Reproduced with permission from ref. 46 Copyright, 2022 Elsevier.)

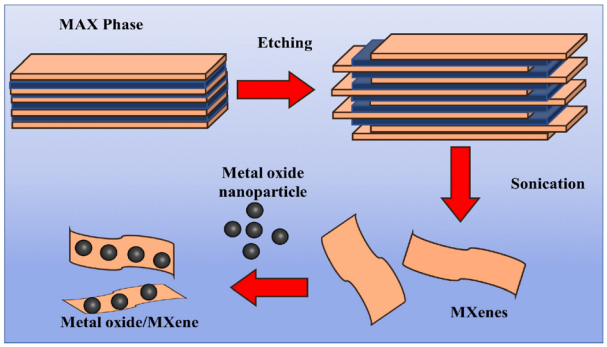

Fig. 7 Schematic illustration of *in situ* growth of metal oxide over MXene nanosheets.

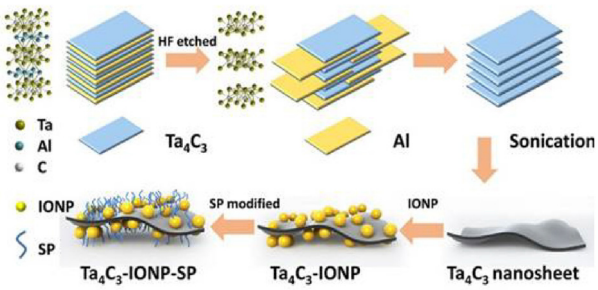

Fig. 8 Schematic illustration of *in situ* growth of iron oxide over Ta_4C_3 MXene. (Reproduced with permission from ref. 91 Copyright, 2018 IVY Spring.)

The kinds of composites reported to date have been synthesized in four ways: (i) *ex situ* mixing, (ii) self-oxidation mixing, (iii) one-step *in situ* growth, and (iv) multistep *in situ* conversion. The choice of an appropriate method varies according to the target material and its precursors. Different synthetic ways result in additional product structures and performances (Table 1).

4. Applications of metal oxide masked MXenes

The enhanced surface area, biocompatibility, hydrophilicity, and strong plasmonic effects of MXenes have gained more attention in biomedical applications. MXenes are widely

Table 1 Advantage and disadvantage of different metal oxide incorporation methods

Methods	Advantages	Disadvantages	Ref.
Co-precipitation	Purity, scalability, versatility, homogeneous incorporation of metal oxides, easy to functionalize with organic and inorganic materials	Limited choice of precursors, challenge to control the layer thickness	128 and 129
Dispersion or mixing	Uniform thickness, high surface area, tunability of size, thickness, surface chemistry, and stability	Solvent selection is critical, reproducibility, time consuming	130 and 131
Facile *in situ* growth	Controlled morphology, homogeneous distribution of metal oxide in MXene matrix, reduced agglomeration, tailored composition	Undesired materials or by products, longer reaction times	132 and 133

employed in biomedical applications such as drug delivery, biosensors, cancer theranostics, and antimicrobial activity. The incorporation of metal oxides has enhanced the catalytic, photothermal, therapeutic, and diagnostic performance of MXenes. This section discusses the antibacterial, anticancer, and sensing applications of metal oxide-masked MXenes.

4.1 Anti-bacterial activity

2D nanosheets of MXenes exhibit anti-bacterial activity owing to their high surface area, hydrophilicity, and negatively charged surface.[71] As it has smaller electrons at the Fermi level, incorporating metal oxide can increase the number of electrons. The surface of MXene has the dexterity to accept electrons from the metal oxide resulting in a substantial number of electrons that ease the charge transfer between bacterial cell walls. The formation of MXene-based heterostructures like $NiFe_2O_4/Ti_3C_2$ (NiFe) proved their anti-bacterial activity against Gram-negative *E. coli* bacteria using the colony count method. It is revealed that NiFe/MXene composite phases showed the best anti-bacterial performance compared to individual NiFe and MXene flakes. The addition of NiFe facilitated a cross-linked network, high surface area, and enhanced magnetic properties.[58]

The same Ti_3C_2 is also anchored with cuprous oxide (Cu_2O) for analyzing photocatalytically triggered anti-bacterial activity.[64] The anti-bacterial studies shown in Fig. 9 revealed that the Cu_2O/MXene nanosheet exhibits excellent anti-bacterial activity against *S. aureus* and *P. aeruginosa* in comparison with MXene, Cu_2O, and their mixture (MXene and Cu_2O), thus resulting in the admirable increase in the bacteriostasis efficiencies to around 97.04% and 95.59% against both the bacteria, respectively.

The abundant electrons on the surface of MXene accepted from Cu_2O facilitated better charge transfer between bacteria and Cu_2O/MXene nanosheets, revealing the synergistic effect of Cu_2O and the bacteriostatic action of MXene. The production of reactive oxygen species responsible for the damage of bacterial cell membranes and cell death was analyzed by photocatalytically triggered anti-bacterial activity. The Cu_2O/MXene induced by sunlight decreases the number of bacterial colonies by generating reactive oxygen species (ROS), which can ruin cell membranes and eventually cause cell death by oxidative stress. It is proved that Cu_2O/MXene produced greater ROS than Cu_2O. Hence, the separation efficiency of photoinduced charges of Cu_2O was significantly ameliorated by combining with MXene nanosheets as a heterojunction

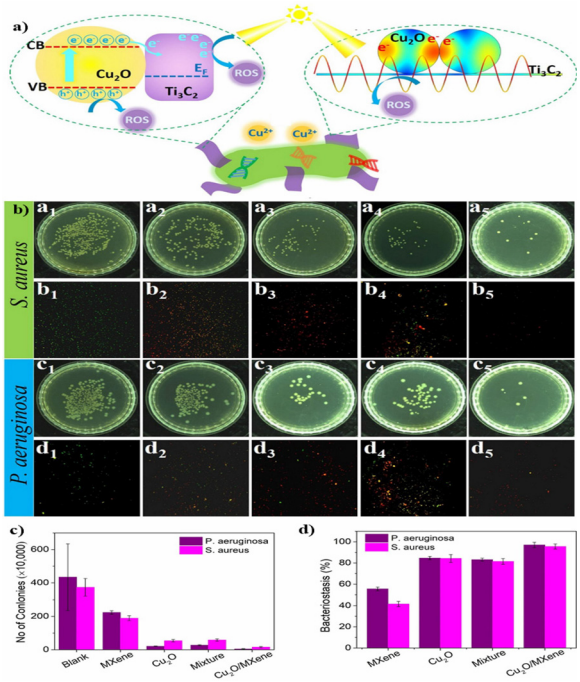

Fig. 9 Schematic representation of light induced antibacterial activity mechanisms and therapeutic effects of Cu_2O/Ti_3C_2 (A–C). (a) Mechanism of optical antibacterial action; (b) profiling of antibacterial activity on *S. aureus* and *P. aeruginosa*; and (c) quantified therapeutic efficiency; (d) bacteriostasis percentage. (Reproduced with permission from ref. 64 Copyright, 2020 Elsevier.)

structure. It is due to the transfer of a photoinduced electron from Cu_2O to MXene, which suppressed the recombination of electron–hole pairs because the Fermi potential level of the MXene (0.71 V *vs.* NHE, pH = 7) was substantially lesser than the conduction band of Cu_2O (−0.703 V *vs.* NHE, pH = 7). Moreover, the MXene grabbed more electrons on the surface from Cu_2O, facilitating the charge transfer between bacteria and Cu_2O/MXene nanosheets. The accumulated charges of intracellular ROS, including hydrogen peroxide (H_2O_2), superoxide anions (O_2^-), or hydroxyl radicals (–OH), resulted in cell membrane damage and cell death.

Excitingly, studies have shown that the incorporation of different structures of metal oxides on MXenes can alter their anti-bacterial activity.[72] For that, the anti-bacterial action of randomly oriented (*i.e.*, dispersed flower-like MnO_2 and MoS_2) *versus* vertically aligned MnO_2 and MoS_2 nanomaterials grown individually on GO, rGO, and Ti_3C_2 MXene substrates (*i.e.*,

MnO_2/GO, MoS_2/rGO, and MoS_2/MXene) against both Gram-positive and Gram-negative bacteria was studied. It has been proven that the sharp edges of 2D nanosheets play a role in targeting and ruining the bacterial cell wall, resulting in the loss of membrane integrity and, eventually, bacteria death.[73] This study was intended to evaluate the impact of 2D nanosheets on the peptidoglycan mesh (PM) in the bacterial cell wall. It was revealed that vertically aligned 2D nanosheet motifs show a higher anti-bacterial activity against both bacteria classes than 2D nanomaterials.[72] To uphold the structural importance of metal oxide masked MXenes in optical-based anti-bacterial applications, a multifunctional hydrogel scaffold is developed using polyethyleneimine grafted Pluronic F127 (F127-PEI) and oxidized sodium alginate and incorporated MXene@CeO_2 nanocomposites and the anti-bacterial activity against both Gram-positive and Gram-negative bacteria is evaluated. The incorporation of MXene@CeO_2 nanocomposites contributed to exquisite antimicrobial efficiency in the multifunctional hydrogen scaffold (FOM) group, revealing a 100% reduction of the bacterial colonies. It is mentioned that the cationic PEI in the FOM attracted the negatively charged bacterial cell membrane, disrupting transmembrane potential, and inducing cell death. Furthermore, incorporating "nano-knife" like MXene@CeO_2 nanocomposites broke the integrity of the cell membrane and resulted in synergistic inhibition of bacterial growth.[74]

Alternatively, ceramic oxide and noble metal nanoparticles are also incorporated over MXene to enhance the optical characteristics of MXene in killing bacteria.[75] In advance, Ti_3C_2 MXene was modified with Al_2O_3/Ag, SiO_2/Ag, and SiO_2/Pd nanoparticles. The bioactivities of Ti_3C_2 MXene, Ti_3C_2/Al_2O_3/Ag, Ti_3C_2/SiO_2/Ag, and Ti_3C_2/SiO_2/Pd nanocomposites were analyzed qualitatively by an agar diffusion method against both Gram-negative (*Escherichia coli*) and Gram-positive bacteria (*Bacillus* sp., *Staphylococcus aureus*, and *Sarcina lutea*). The anti-bacterial studies in Fig. 8 revealed that the modification of Ti_3C_2 MXene with Al_2O_3 + Ag, SiO_2 + Ag, and SiO_2 + Pd resulted in significantly increased anti-bacterial properties; the results of the experiment with *Staphylococcus aureus* with the application of the dilution method revealed that all the tested samples were able to inhibit the growth of potentially pathogenic bacterial strains. The considered mechanism of action for Ti_3C_2 MXene is related to the direct physical interactions between the edges of the nanosheets and the bacterial cell wall or the membrane surface. As a result, cells lose their integrity, and the internal cytoplasm is released together with DNA.

Cong Liu *et al.*[63] integrated a covalent organic framework with MXene structures, anchored Cu_2O nanoparticles on the surface of Ti_3C_2. The prepared Ti_3C_2/$TpPa^{-1}$/Cu_2O systems exhibited anti-bacterial activity against *S. aureus* and *P. aeruginosa*. It is reported that the enhancement of anti-bacterial activity is because the synergistic effect of Ti_3C_2/$TpPa^{-1}$/Cu_2O; $tppa^{-1}$ increased the contact range with bacteria and killed bacteria by generating ROS as it has a vast surface area. Ti_3C_2 assisted the flow of carriers between layers, which improved the separation efficiency of electron–hole pairs and caused more ROS generation. Besides, copper ions released by Cu_2O denatured the bacterial DNA and exhibited toxicity to bacteria. Rather than Cu_2O metal oxide, recently, CuO was masked over Ti_3C_2 by the ultrasonication route for photocatalytic anti-bacterial applications.[46] It is revealed that the anti-bacterial activity of CuO/MXene is due to the vital force of attraction generated between the negatively charged bacterial cell membrane and positively charged heavy metal ions present on the sample surface. After penetrating the cell membrane, heavy metal ions react with proteins containing thiol (–SH) groups and inactivate the protein resulting in the death of bacteria. Under the metal oxide section, some rare-earth metal-based oxides are also masked on the surface of MXene. As a promising metal oxide gadolinium (Gd^{3+}) doped V_2O_5 (GVO), nanostructures with MXenes are demonstrated to have an anti-bacterial effect on both Gram-positive (*S. aureus*) and Gram-negative (*P. vulgaris*) strains.[76] GVO/MXene creates reactive oxygen species (ROS) in the presence of light and causes the eradication of RNA, resulting in the death of bacterial strains. It is demonstrated that the efficiency of the prepared nanocomposites was higher than that of the individual nanoparticle. Akin to this, WO_3/MXene nanocomposites also presented as photoinduced anti-bacterial agents against the Gram-positive strain *S. aureus* and Gram-negative strains *E. coli*, *Pneumonia*, and *P. vulgaris* and demonstrated better activity against the Gram-positive strain *S. aureus*. The WO_3/MXene composite showed good activity at a low concentration against pneumonia in Gram-negative strains. It is stated that the WO_3/MXene composite does not exhibit anti-bacterial activity against *E. coli* and *P. vulgaris*, whereas WO_3 and MXene showed good anti-bacterial activity. It is reported that the zero anti-bacterial activity against *E. coli* bacteria and *P. vulgaris* is due to an extra outer membrane that increased the resistance to the WO_3/MXene composite. The increased concentration of composites also decreased the anti-bacterial activity owing to the size and agglomeration. $CuFe_2O_4$/MXene nanohybrids are also employed for evaluating the anti-bacterial activity against *E. coli*, *Pseudomonas aeruginosa*, *Klebsiella pneumonia*, *Proteus vulgaris*, and *Staphylococcus aureus*. The anti-bacterial studies revealed that composites developed better anti-bacterial performance than individual nanoparticles. It is reported that the anti-bacterial activity is due to the interaction of the positively charged metal particles with the negatively charged bacterial cells.[69] Unlike metal oxide alone, carbon-based graphite is also used in a hybrid metal oxide–carbon–MXene structure against photocatalytic and bacteriostatic applications. For example, TiO_2 is supported with graphite over Ti_3C_2 MXene, and the hybrid nanostructures revealed exquisite anti-bacterial efficiency against *E. coli*. The nanostructures expressed anti-bacterial activity under light exposure owing to the excessive radicals that cause oxidative stress in bacterial cells. It is reported that controlled oxidation of delaminated MXene structures contributes to anti-bacterial activity and assembly of hybrid nanostructures (TiO_2–Ti_3C_2) with graphitic carbon persuaded the generation of oxidative stress in bacteria to promote cell lysis.[77] List of various metal oxide-masked MXene in anti-bacterial applications is detailed in Table 2.

Table 2 Summary of various metal oxide masked MXenes in anti-bacterial applications

S. no.	Metal oxide	MXene	Bacteria	Remarks	Ref.
1	$NiFe_2O_4$	Ti_3C_2	*Escherichia coli* (*E. coli*)	NiFe/MXene exhibited excellent antibacterial activity against Gram negative *E. coli* bacteria	58
2	Cu_2O	Ti_3C_2	*Staphylococcus aureus* (*S. aureus*) and *P. aeruginosa*	Ti_3C_2/$TpPa^{-1}$/Cu_2O nanocomposites demonstrated good antibacterial activity of 98.90% and 99.62%, and enhanced by 50% and 33% when compared to pure $TpPa^{-1}$-COF	63
3	MnO_2	Ti_3C_2	*Bacillus subtilis* and *E. coli*	Vertically aligned 2D MnO_2 nanosheets on grapheme oxide and Ti_3C_2 Mxene revealed maximal antimicrobial activity, signifying that the edges of the nanosheets weakens the bacterial cell	72
4	CeO_2	Ti_3C_2	*E. coli* (Gram-negative bacteria), *S. aureus* (Gram-positive bacteria)	MXene@CeO_2 nanocomposite based multifunctional hydrogel exhibited distinct antibacterial behaviour against *E. coli*, *S. aureus*, MRSA and showed 100% reduction in bacterial colonies	74
5	SiO_2	Ti_3C_2	*E. coli*, *Sarcina lutea*, *S. aureus*, and *Bacillus* sp.	NiFe/MXene exhibited excellent antibacterial activity against Gram negative *E. coli* bacteria	75
6	TiO_2	Ti_3C_2	*E. coli*	TiO_2–$Ti_3C_2T_x$ killed 97% *E. coli* bacteria under light exposure by producing the excessive radicals that cause oxidative stress on bacterial cells	77
7	Cu_2O	Ti_3C_2	*S. aureus* and *P. aeruginosa*	Cu_2O/MXene nanocomposite displayed good antibacterial activity against *S. aureus* and *P. aeruginosa* with the bacteriostasis efficiency of 97.04% and 95.59%, respectively	63
8	WO_3	Ti_3C_2	*S. aureus*, *E. coli*, *K. pneumonia*, *P. vulgaris*	WO_3/MXene nanocomposite expressed good antibacterial activity due to the electrostatic attraction between the nanocomposite and the bacterial cell membrane	45
9	$CuFe_2O_4$	Ti_3C_2	*E. coli*, *Pseudomonas aeruginosa*, *Klebsiella pneumonia*, *Proteus vulgaris* and *S. aureus*	$CuFe_2O_4$/Ti_3C_2 composites showed good antibacterial activity due to the addition of $CuFe_2O_4$	69

4.2 Anti-cancer activity

Cancer is a necrotic epidemic disease with no specific treatment. Massive research has been in progress, working on cancer therapy for decades, with some improvement, yet many drawbacks persist. Conventional treatments like surgery,[78] chemotherapy,[79] and radiation therapy[80] are the most used treatments;[81] they exhibit several limitations, like incomplete removal of tumors, damage to healthy tissue, hair loss, nausea, and bowel issues. To conquer these barriers, nanomaterials were predominantly studied as a targeted drug delivery method for cancer therapy.[82,83] One of these materials is Ti_3C_2, also known as MXene, a 2D material studied for many biomedical applications, tumor detection (*i.e.*, as contrast agents), cancer therapy, and drug delivery.[84] MXenes are endowed with the following beneficial properties suitable for cancer therapy. (i) In the presence of functional groups, such as –OH, –O, or –F, MXenes are hydrophilic in nature,[24,26] which is favourable for surface modification. (ii) The large surface area makes the MXene host massive molecules for synergistic therapy, including immune adjuvants,[85] photosensitizers (PS),[86] and chemotherapeutic drugs.[87] (iii) Several compositions of MXenes, including Ti_2C, Ti_3C_2, Nb_2C, and Mo_2C, have been tested to be non-toxic and biocompatible with living organisms. Excellent biocompatibility might be due to the metal in the "M" layer, like Ti, Mo, and Nb, being relatively inert to living organisms. Other significant elements, such as nitride and carbon, are essential in the structure of biological organisms. (iv) They exhibit substantial plasmonic effects in the NIR region, making them more favourable for both *in vivo* photothermal (PTT) and photoacoustic (PA) imaging in the first or the second biological window. Therefore, MXenes were studied by many researchers for cancer photothermal therapy by killing cancer cells by heat, leading to protein denaturation and cell death.[88] It was reported that MXenes with a size of around 180 nm could explicitly target and reach the cancerous microenvironment by enhanced permeability and retention of EPR.[89] Although MXenes showed good photothermal efficiency that makes them a potential candidate for photothermal therapy, the internalization of MXenes into cancer cells was not studied extensively.

Lin *et al.*[90] applied MXenes to treat tumors using PTT for the first time. Typical representatives of MXenes, such as Ti_3C_2, Nb_2C, Ta_4C_3, and Ti_2C, are endorsed to have excellent photothermal properties and are used in PTT. Using Ti_3AlC_2 powder as the raw material, the 2D nanosheets of Ti_3C_2 were functionalized with soybean phospholipid (SP) for high-efficiency PTT of tumors. It is revealed that introducing SP enhanced the stability of Ti_3C_2 nanosheets in various dispersions and improved their applicability in tumor diagnosis and treatment. Furthermore, the composite nanosheet Ti_3C_2–SP had excellent PTT performance, as Ti_3C_2–SP at a low concentration of 72 μg ml^{-1} could be heated to above 55 °C in 6 min, which fulfilled the temperature requirements of PTT for the ablation of tumor tissue. Zhuang Liu *et al.*[91] prepared (Ta_4C_3)-based MXene nanosheets anchored with iron oxide nanoparticles modified using soybean phospholipid (SP) to increase the stability. The prepared Ta_4C_3–IONP–SPs were evaluated for MR/CT dual-modality imaging and photothermal hyperthermia of breast cancer. Without NIR radiation, the prepared Ta_4C_3–IONP–SP nanosheets failed to exhibit cytotoxicity on breast 4T1 cancer cells at different concentrations (0, 12.5,

25, 50, 100, 200 ppm). Upon NIR radiation for 5 min at the power density of 1.5 W cm^{-2}, the photothermal-killing effect was observed with increased Ta_4C_3–IONP–SP concentrations, where more cancer cells were ablated and then killed under NIR irradiation. The therapeutic efficacy of the Ta_4C_3–IONP–SP MXene *in vivo* was determined in 4T1 tumor-bearing mice and is represented in Fig. 10. It is observed that the temperature of the tumors from mice in post-injection of Ta_4C_3–IONP–SPs increases from about 34 °C to 48 °C within 10 min, which is adequately high to ablate cancer cells and tumor tissues. Two days after photothermal hyperthermia, the initial tumors disappeared in the group injected with Ta_4C_3–IONP–SPs under laser irradiation, leaving black scars at tumor sites. It was found that around 1.02% Ta_4C_3–IONP–SPs accumulated in the tumor tissue passively due to the EPR effect. Retention of Ta_4C_3–IONP–SPs in the liver and spleen may be associated with the significant macrophage uptake of nanoparticles in reticuloendothelial systems. Primarily, the high photothermal-conversion efficiency of Ta_4C_3–IONP–SP composite nanosheets (η: 32.5%) has accomplished complete tumor eradication without reoccurrence, demonstrating the highly efficient breast-tumor hyperthermia performance.

2D niobium carbide (Nb_2C) MXene was first reported by Huijing Xiang *et al.*[92] *via* a two-step chemical exfoliation strategy for photothermal conversion in the NIR-II bio window, which demonstrated excellent *in vivo* photothermal ablation capability in the NIR-II bio window. The Nb_2C@$mSiO_2$ nanosystem reported by the same group was loaded with AIPH

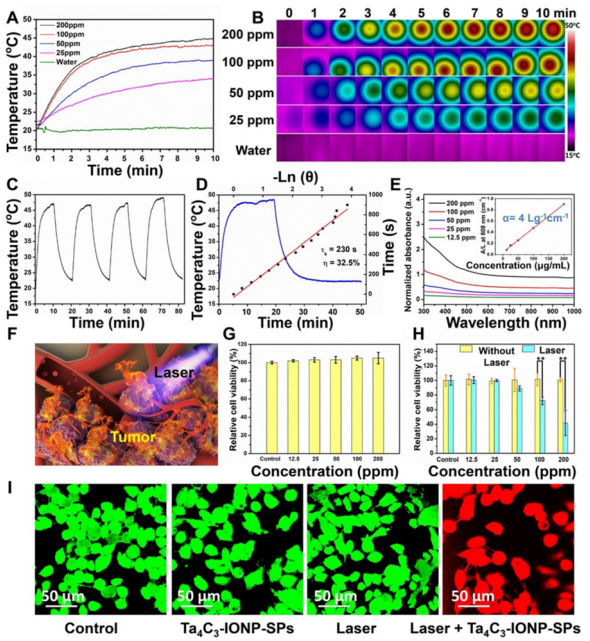

Fig. 10 (A) Photothermal and therapeutic evaluation profiles of Ta_4C_3–IONP–SPs under a laser, (B) the corresponding infrared thermal images. (C) Heating/cooling, (D) temperature-changing profile, (E) UV-vis spectra and (F) 3D-schematic illustration of Ta_4C_3–IONP–SPs as PTAs for 4T1 cells. (G) Relative viability and (I) confocal fluorescence images. (Reproduced with permission from ref. 91 Copyright 2018, IVY Spring.)

molecules as the free-radical source. Upon 1064 nm NIR-II laser irradiation, the heating of nanoparticles (NPs) triggered the rapid release and decomposition of encapsulated initiators to generate free radicals independent of oxygen levels, resulting in significant *in vitro* cell apoptosis and *in vivo* tumor eradication, which is herein regarded as the cancer-therapeutic modality of "thermodynamic therapy". The synergistic therapeutic efficiency of the photothermal effect was exhibited. Dong Yang Zhang *et al.*[93] prepared TiO_{2-x} decorated titanium carbide MXene for photoacoustic/photothermal bimodal imaging guided near-infrared II (NIR-II) photothermal enhanced SDT of the tumor.

Upon ultrasound/NIR-II radiation, Ti_3C_2@TiO_{2-x} nanoplatform provoked substantial cellular killing *in vitro* and complete tumor eradication *in vivo* without recurrence of tumors and systemic toxicity. MXene-based multifunctional composites, Fe_3O_4/MnO_x–Nb_2C, were employed for the tumor-responsive *T*1 and *T*2 MRI-guided photothermal ablation of breast cancer in the NIR-II biowindow. The Fe_3O_4 composites act as *T*2 contrast agents for *T*2-weighted MR imaging. This composite nanosheet was modified with soybean phospholipid to enhance the stability, biosafety in physiological environments, and long circulation time. It is reported that the high photothermal-conversion efficiency of Fe_3O_4/MnO_x–Nb_2C composite MXenes (η = 30.9%) dexterously ablated tumor cells without further reoccurrence both *in vitro* and *in vivo* after laser irradiation in the second biological window (NIR-II, 1064 nm).[94] Two-dimensional tantalum carbide was employed for the photothermal cancer ablation. Manganese oxide nanoparticles were grown on the surface of Ta_4C_3 by the redox reaction between the MXene surface and strongly oxidative MnO_4, and the surface of the MXene composites was modified with soybean phospholipid to enhance biosafety. The composite exhibited good photothermal conversion efficiency for ablating the tumor cells and acted as a contrast agent. It is indicated that tantalum-based and MnO_x components in the prepared composites acted as high-performance contrast agents for simultaneous computed tomography and *T*1-weighted magnetic resonance imaging, respectively. It is revealed that the composites showed significant tumor growth suppression by photothermal hyperthermia.[70] MXene composites and metal oxide composites were utilized for magnetic hyperthermia. Using the redox reaction-induced growth, MnO_x was grown on titanium carbide MXene sheets. The incorporation of MnO_x on the surface of nanosheets acts as the pH-responsive contrast agent for *T*1-weighted MR imaging. Simultaneously the ultrathin Ti_3C_2 nanosheets revealed high photothermal-conversion performance for efficient thermal ablation of tumors *via* PTT.[90] A summary of various metal oxide-masked MXenes in anti-cancer activities is listed in Table 3.

4.3 Sensing applications

The unique physical, chemical, and ion transport properties of MXenes make them an excellent choice in many applications, exclusively in sensing[95,96] and biosensing.[97–99] MXenes feature excellent biocompatibility and allow secure immobilization of

Table 3 Summary of various metal oxide masked MXenes in cancer therapeutics

S. no.	Metal oxide	MXene	Light	Power	Summary	Ref.
1	Iron oxide	Ta_4C_3	NIR I	1.5 W cm^{-2}	Ta_4C_3–IONP–SPs composite MXenes achieved complete tumor eradication with high photo-thermal-conversion efficiency (η: 32.5%)	124
2	SiO_2	Nb_2C	NIR II	1 W cm^{-2}	SiO_2/Nb_2C MXene showed that a better photothermal-conversion effect provoked cancer cell apoptosis	92
3	TiO_2	Ti_3C_2	NIR II	1 W cm^{-2}	Titanium carbide, Ti_3C_2 showed good photothermal efficiency and demonstrated complete tumor elimination in 4T1 tumor bearing mice	93
4	Fe_3O_4	Nb_2C	NIR II	1.5 W cm^{-2}	Fe_3O_4/MnO_x–Nb_2C composite nanosheets expressed high photothermal-conversion efficiency in the NIR-II biowindow (1064 nm, η 30.9%)	94
5	MnO_x	Ti_3C_2	NIR I	1 W cm^{-2}	MnOx/Ti_3C_2 composite MXenes exhibited excellent contrast-enhanced PA-imaging properties and demonstrated efficient tumor ablation and tumor-growth suppression	90

enzymes and proteins on their surface.[100–102] They possess a large specific surface area, anisotropic charge carrier conductivity, environmental friendliness, and excellent chemical stability.[103] Surface dangling bonds enable MXenes to attract various functional groups, making them unique for sensing applications. Metal oxides are used to fabricate a heterostructure or composite with MXenes to enhance sensing quality. Metal oxides have various beneficial properties like high thermal and chemical stability,[33] substantial mechanical strength,[104] sizeable piezoelectric coefficient,[105] high exciton binding energy, and optical gain,[106] making them an ideal material for the sensor.[107]

As depicted in Fig. 11,[108] hybrid composites as heterojunctions using partially-oxidized Ti_3C_2 sheets and photo-active $NiWO_4$ nanoparticles (NPs) are prepared for selective sensing of prostate-specific antigens (PSA). Electrocatalytic and photoelectrochemical (PEC) studies revealed a remarkable electrochemical response, with a redox couple shift to 0.27 V/0.15 V and a two-fold rise in the measured current output (1.2 μA). It is mentioned that the predominant performance of MX–$NiWO_4$ is due to the increased surface area, high conductivity of Ti_3C_2, and exposed surface-active sites of MX–$NiWO_4$. The ideal interfacial arrangement of MX–$NiWO_4$ assisted in the electrocatalytic mechanism-based PEC immuno-sensing of PSA. The developed PEC biosensor's detection range was from 1.2 fg mL^{-1} to 0.18 mg mL^{-1} with a detection limit of 0.15 fg

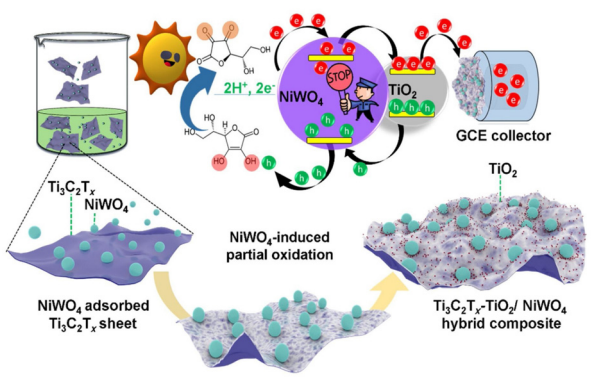

Fig. 11 Schematic illustration of mechanisms of surface adsorption of $NiWO_4$ NPs over ultra-thin $Ti_3C_2T_x$ sheets. (Reproduced with permission from ref. 108 Copyright 2022, Elsevier.)

mL^{-1}. In another study,[109] a TiO_2/Ti_3C_2/Cu_2O heterostructure was fabricated by *in situ* generations of TiO_2 NPs on Ti_3C_2 MXenes and the introduction of Cu_2O *via* a one-step hydrothermal reaction. The impact of Ti_3C_2, as a mediator between TiO_2 and Cu_2O, adequately accelerated the charge transfer and prolonged photoelectrons lifetime, which made the fabricated sensor extremely sensitive and conductive. It is proven that heterojunction demonstrated good PEC activity with dissolved O_2 as electron scavengers, during which H_2O_2 is produced as an intermediate to further trap the photogenerated electrons. Glucose detection was observed in the change in the photocurrent of TiO_2/Ti_3C_2/Cu_2O, decreasing photocurrent with the increased glucose concentration in a wide range from 100 nM to 10 μM with a low detection limit of 33.75 nM (S/N = 3).

To uphold the superior sensing characteristics of MXenes, metal oxide-based MXene heterojunctions[67] are fabricated by electrospinning $FeWO_4$ bimetallic nanofibers tagged on delaminated single-layered Ti_3C_2 MXenes for the detection of rutin. The heterostructure revealed favourable electrocatalytic properties for rutin oxidation due to its electroactive interconnecting network of single-layered MXene with metal-oxide fibers having high defective edge/plane sites. Compared to bare glassy carbon electrodes (GCE) and composites, the prepared structures exhibited superior performance. Volumetric studies of the fabricated heterostructure displayed an ultralow detection limit of 0.42 nM, an ultrawide linear determination range from 4 to 147 nM, and a high sensitivity of 0.3799 μA nM^{-1} cm^{-2}. The electrochemical studies of the MXene–$FeWO_4$ nanocomposite showed favourable stability and persistent anti-interference ability. The prepared nanocomposite revealed excellent activity in detecting RT in human serum, orange juice, and black tea samples.

Interestingly, hybrid combinations of[110] titanium dioxide/MXene and polyvinyl alcohol/graphene oxide (TiO_2/MXene–PVA/GO) composites are prepared to modify a screen-printed carbon electrode (SPCE) for urinary norepinephrine (NE) detection. The as-prepared composite substantially upgraded the sensor performances due to the favourable electrocatalytic activity of TiO_2, high conductivity of MXene, and auto-sample preconcentration *via* the PVA/GO hydrogel. Cyclic voltammetry and amperometry studies revealed that the composites expressed their electrochemical response at +0.4 V, and oxidation of NE is proportional to NE. The contribution of the

Table 4 Summary of various metal oxide masked MXenes in sensor applications

S. no.	Metal oxide	MXene	Analyte	Remarks	Ref.
1	$NiWO_4$ & TiO_2	Ti_3C_2	Prostate-specific antigens	$Ti_3C_2T_x$–TiO_2/$NiWO_4$ hybrid composite showed photoelectrochemical sensing of prostate specific antigen, over a wide detection range from 1.2 fg mL^{-1} to 0.18 mg mL^{-1}, with a detection limit of 0.15 fg mL^{-1}	108
2	TiO_2	Ti_3C_2	H_2O_2	TiO_2 nanoparticle modified Ti_3C_2 MXene nanocomposite used for the detection of H_2O_2 with a low detection limit of 14 nM, a wide linear range of 0.1–380 μM for H_2O_2, and especially, an excellent long-term stability	111
3	TiO_2/Cu_2O	Ti_3C_2	Glucose	The TiO_2/$Ti_3C_2T_x$/Cu_2O composite was probed as a photoelectrochemical sensing system for glucose detection in a linear range from 100 nM to 10 μM with a low detection limit of 33.75 nM	109
4	$FeWO_4$	Ti_3C_2	Rutin	The MXene/$FeWO_4$ composite showed excellent selectivity for Rutin detection among a series of interfering ions and biomolecules	67
5	TiO_2	Ti_3C_2	Norepinephrine	The TiO_2/MXene–PVA/GO based hydrogel used for the detection of norepinephrine with a detection limit (3σ) of 6 nM	110
6	TiO_2	Ti_3C_2	Glucose	TiO_2–Ti_3C_2 was employed as an electrogenerated chemiluminescence biosensor for the detection of glucose in the wide concentration range of 20 nM–12 mM with a low detection limit of 1.2 nM	125
7	TiO_2	Ti_3C_2	Dopamine & uric acid	TiO_2/Ti_3C_2 demonstrated good selectivity and reproducibility for dopamine and uric acid detection in urine and serum samples with recoveries of 98.4 to 100.9%	112
8	TiO_2	Ti_3C_2	Glutathione	The TiO_2/Ti_3C_2 heterostructure film exhibited high stability, sensitivity, and selective detection of glutathione	126
9	ZnO	Ti_3C_2	Glucose	ZnO/MXene was employed to prepare a skin-attachable and stretchable electrochemical enzymatic sensor for the detection of glucose and exhibited enhanced sensitivity in sweat samples (29 μA mM^{-1} cm^{-2}), low limit of detection (LOD ≈ 17 μM), and a broad linear detection range (LDR = 0.05–0.7 mM) that satisfies glucose detection application in human sweat	127

PVA/GO hydrogel is shown in the increased surface area and sample volume absorption, increasing sensor electrochemical signals and sensitivity.

Similarly,[111] TiO_2 nanoparticle-modified organ-like Ti_3C_2 MXene (TiO_2–Ti_3C_2) nanocomposite is used to immobilize hemoglobin (Hb). Spectroscopic and electrochemical studies demonstrated that the TiO_2–Ti_3C_2 nanocomposite is an excellent immobilization matrix biocompatible with redox proteins, affording good protein bioactivity and stability. The direct electron transfer of Hb due to the unique organ-like hybrid structure of TiO_2–Ti_3C_2 improved the detection of H_2O_2 with a wide linear range of 0.1–380 μM for H_2O_2 (sensitivity of 447.3 μA mM^{-1} cm^{-2}), and a meager detection limit of 14 nM for H_2O_2. It is reported that incorporating TiO_2 nanoparticles enhanced biocompatibility, bioactivity, and prolonged stability. In addition to TiO_2, masked MXene sensors,[112] TiO_2/Ti_3C_2 nanocomposite, along with covalent organic polymers (NUF), are prepared for the detection of dopamine (DA) and uric acid (UA). The differential pulse voltammetry studies revealed that TiO_2/TiCT/NUF expressed high sensing activity with low detection limits of 0.2 and 0.18 nM (S/N = 3) in the concentration ranges from 0.002 to 100 μM and 0.001 to 60 μM for simultaneous determination of DA and UA, respectively. The simultaneous detection is achieved due to the abundant redox sites, large electroactive area, and heterostructure's enhanced electron capacity. Different combinations of metal oxide masked MXenes for sensor applications are listed in Table 4.

4.4 Other biomedical applications

Like other fascinating applications, tissue engineering and regenerative medicine also extended the fields of MXenes due to their remarkable features like conductivity, large surface area, hydrophilicity, two-dimensional geometry, and particle size regulation. MXenes combined with polymers and hydrogels are widely explored in tissue engineering, regenerative medicine and wound dressing because of their immunomodulatory and anti-inflammatory properties.[113,114] Jacek Wychowaniec *et al.* developed an rGO–MXene hydrogel as a cellular network for tissue engineering applications. It is reported that the rGO-based hydrogel without MXene had a hydrophobic surface with an elastic modulus of 40k Pa and rGO–MXene-based hydrogel expressed a hydrophilic surface, softer with an elastic modulus of 20 kPa. MXene Ti_2C, along with cryogen, was reported for cardiac tissue engineering, *i.e.* Ti_2C proportion provided enough mechanical properties and an appropriate conductivity to match the natural myocardium and promoted the repair of myocardial infarction. MXenes are used in wound healing along with hydrogels under electric stimulation as they have the ability to enhance the electrophysiological properties of wound dressing materials.[115,116] Besides, MXene coupled with CeO_2-based nanozyme was reported to have a synergistic effect in hyperthermia-enhanced tumour nano catalytic therapy.[117] Though MXenes were employed in all these applications, metal oxide-masked MXenes have not been explored much.

As described above, various metal oxides were utilized for effectively improving the optical properties of MXenes for various biomedical applications. However, depending on the metal oxide type, the applications vary. For example, TiO_2 is a known photocatalyst and is effectively utilized for various ROS-generating applications, such as anti-bacterial and anti-cancer, since its Ti^{2+} ionic form exhibits ROS-generation activities.

Similarly, copper and cobalt-masked MXenes are also used since they help generate ROS in the presence of external light. On the other hand, metal oxides such as cerium and manganese exhibit concentration-dependent ROS scavenging activities; these nanoformulations were used in anti-oxidant applications. So, the type of application was determined by the type of metal oxide incorporation.

5. Scope and perspectives

MXenes have attractive and tunable properties, but limitations like easy oxidation and restacking are encountered. In the context of MXenes and metal oxide incorporated MXenes, stability issues often arise due to their sensitivity to oxidation. The terminal surface functional groups of MXenes (–OH, –F) are particularly susceptible to oxidation. The high reactivity of MXenes, coupled with the presence of defects and impurities, may contribute to this lack of stability. Additionally, improper mixing of metal oxides with MXenes can result in a lack of structural stability. To enhance and improve the stability of MXenes and metal oxide incorporated MXene, various approaches can be employed, including surface modifications, protective coatings, and suitable composites.

Overcoming these limitations is crucial to exploring the optical properties of MXenes for biomedical applications. Metal oxides have a high surface area, biocompatibility, interesting redox, catalytic, and semiconducting activity, and good mechanical stability. The use of metal oxide masked MXenes for clinical applications is still growing. Some studies and factors must be explored for improved diagnostic and therapeutic applications. (i) Enhancing biocompatibility, including biodegradability, biodistribution, and toxicity, using the incorporation of metal oxides based on surface modification, concentration, and structure. (ii) The interaction between metal oxide masked and biological organisms, *i.e.*, the immunological effect of MXenes and the immune system, *in vivo* studies need to be conducted to optimize the size, shape, surface, and physical and chemical properties of metal-oxide masked MXenes. (iii) The incorporation or encapsulation of the drug in metal oxide masked MXenes, and their performance must be studied for theranostic applications. (iv) Optimizing the optical properties and catalytic reactions of MXenes using metal oxides must be explored widely for enhancing the sensing applications. (v) The impact of incorporating different structures of metal oxides like rods, spheres, sheets, and quantum dots towards clinical applications can be prioritized in future research. More research will develop a different combination of metal oxide-masked MXenes to enhance diagnostic and therapeutic performances. With the exceptional properties of MXenes and the potential of metal oxides, enormous improvement can be implemented in developing cancer therapies, drug delivery platforms, biosensors, and bioelectronics.

Like most inorganic nanosystems, the poor biodegradability of 2D MXene nanosheets is the pivotal issue, which may hinder their further oncological research and clinical translation. Therefore, it is essential to systematically evaluate the biodegradation performance of MXene nanosheets in a complex physiological environment. To date, several MXenes have undergone individual studies and case-by-case phenomenon evaluations, including Ti_3C_2,[118] Ta_4C_3,[119] Nb_2C,[120] MoC_2,[121] V_2C,[122] and TiN.[123] However, the biological effects of MXenes are only preliminarily assessed at the cellular and animal level. Currently, reliable data on the long-term biological effects and biosafety are still highly lacking, which requires further systematic and in-depth evaluation and assessment. Although many studies have demonstrated the great potential of MXenes in biomedical applications, their clinical translation is still in its infancy. Therefore, the systematic investigation of the interaction between MXenes and biological microenvironments should be systematically investigated in the following fundamental research.

Additionally, the effect of surface functionalization on the biological behavior of MXenes requires further investigation. Significantly, the scale-up fabrication of 2D MXenes is a significant aspect for their design and engineering. A further and deeper exploration of materials science and clinical translation requires cooperation among researchers of interdisciplinary and industrial sectors. It is highly expected that the development of nanotechnology and bioscience will achieve more fundamental and technological breakthroughs to afford the limitless application of MXenes in varied biomedical areas shortly, provided the challenges facing and critical issues are adequately solved.

6. Conclusion

This review has emphasized the significance of incorporating metal oxides into the MXene framework for biomedical applications. According to the literature survey, metal oxides have played a crucial role in enhancing the high surface area, electrical conductivity, stability, and sensitivity of MXenes. It is evident that the incorporation of metal oxides into the MXene structure holds great promise for future biomedical applications. However, the mechanism of interaction between metal oxides and MXenes is still in its infancy, requiring further investigation. This compilation underscores the need for more research on utilizing metal oxide/MXene nanocomposites for various biomedical applications. The biomedical applications of 2D MXenes face limitations such as easy aggregation, complex surface engineering, inadequate stability, and potential toxicity. Factors such as lateral size, the number of layers, and the degree of oxidation significantly influence degradation and stability during *in vivo* circulation.

The interaction between MXene nanosheets and the physiological environment, the analysis of metabolic pathways, and the potential side effects of MXene nanosheets remain unclear. There exists a notable paradox where rapid degradation may affect our desired therapeutic outcomes while meeting biological safety requirements. Therefore, the appropriate degradation rate should be considered in the design

and synthesis of MXenes to simultaneously pursue ideal therapeutic outcomes and low toxicity.

This review lays a solid foundation for further research by providing technical details and in-depth insights that warrant focused attention. A thorough investigation of these aspects will provide excellent solutions to the challenges faced in biomedical applications. Additionally, further research in the rapid assessment of nanomaterials for biomedical applications within a microfluidic platform is anticipated.

Conflicts of interest

There are no conflicts to declare.

Acknowledgements

The Russian Federation's Ministry of Science and Higher Education provided support for the research, which Dr Rajesh Kumar Manavalan sincerely acknowledges (Ural Federal University project within the Priority 2030 Program) and contract number 40/is2. The authors acknowledge the support and funding from Aaivalayam.

References

1 A. P. Ramos, *et al.*, Biomedical applications of nanotechnology, *Biophys. Rev.*, 2017, **9**(2), 79–89.
2 M. Mabrouk, *et al.*, Nanomaterials for biomedical applications: Production, characterisations, recent trends and difficulties, *Molecules*, 2021, **26**(4), 1077.
3 Y. Gogotsi and B. Anasori, *The rise of MXenes*, ACS Publications, 2019, pp. 8491–8494.
4 K. A. Papadopoulou, *et al.*, A perspective on MXenes: Their synthesis, properties, and recent applications, *J. Appl. Phys.*, 2020, **128**(17), 170902.
5 H. Kaur, *et al.*, Progress and challenges of graphene and its congeners for biomedical applications: Drug delivery, gene delivery, biosensing, bioimaging, and tissue engineering, *J. Mol. Liq.*, 2022, 120703.
6 M. Garg and A. Thakur, A review: Biomedical applications of phosphorene, antimonene, and germanene-based 2D material/hydrogel complexes, *J. Mater. Sci.*, 2022, 1–12.
7 N. Sultana, *et al.*, Synthesis, Modification, and Application of Black Phosphorus, Few-Layer Black Phosphorus (FLBP), and Phosphorene: A Detailed Review, *Mater. Adv.*, 2022, **3**, 5557–5574.
8 D. Presutti, *et al.*, Transition metal dichalcogenides (TMDC)-based nanozymes for biosensing and therapeutic applications, *Materials*, 2022, **15**(1), 337.
9 M. D. Prakash, *et al.*, Performance analysis of ion-sensitive field effect transistor with various oxide materials for biomedical applications, *Silicon*, 2022, **14**(11), 6329–6339.
10 J.-C. Lei, X. Zhang and Z. Zhou, Recent advances in MXene: Preparation, properties, and applications, *Front. Phys.*, 2015, **10**(3), 276–286.
11 S. Panda, *et al.*, MXene based emerging materials for supercapacitor applications: Recent advances, challenges, and future perspectives, *Coord. Chem. Rev.*, 2022, **462**, 214518.
12 V. Natu, *et al.*, Effect of Base/Nucleophile Treatment on Interlayer Ion Intercalation, Surface Terminations, and Osmotic Swelling of $Ti_3C_2T_z$ MXene Multilayers, *Chem. Mater.*, 2022, **34**(2), 678–693.
13 X. Zhang, W. Zhang and H. Zhao, Electrochemical performance of $Ti_3C_2T_x$ MXenes obtained via ultrasound assisted LiF-HCl method, *Mater. Today Commun.*, 2022, **33**, 104384.
14 U. Khan, *et al.*, Synthesis of fluorine free MXene through lewis acidic etching for application as electrode of proton supercapacitors, *J. Alloys Compd.*, 2022, **926**, 166903.
15 H. Chen, H. Wang and C. Li, Mechanically Induced Nanoscale Architecture Endows a Titanium Carbide MXene Electrode with Integrated High Areal and Volumetric Capacitance, *Adv. Mater.*, 2022, **34**(43), 2205723.
16 Q. Tang, *et al.*, Boosted CO_2 photoreduction performance on Ru-Ti_3CN MXene-TiO_2 photocatalyst synthesized by non-HF Lewis acidic etching method, *J. Colloid Interface Sci.*, 2022, **619**, 179–187.
17 J. Chen, *et al.*, Molten Salt–Shielded Synthesis (MS_3) of MXenes in Air, *Energy Environ. Mater.*, 2022, 1–6.
18 I. Ashraf, *et al.*, Hydrothermal synthesis and water splitting application of d-Ti_3C_2 MXene/V_2O_5 hybrid nanostructures as an efficient bifunctional catalyst, *Int. J. Hydrogen Energy*, 2022, **47**(64), 27383–27396.
19 F. Cao, *et al.*, Mixed-Dimensional MXene-Based Composite Electrodes Enable Mechanically Stable and Efficient Flexible Perovskite Light-Emitting Diodes, *Nano Lett.*, 2022, 4246–4252.
20 L. Gao, *et al.*, Optical Properties of Few-Layer Ti_3CN MXene: From Experimental Observations to Theoretical Calculations, *ACS Nano*, 2022, **16**(2), 3059–3069.
21 B. Zhu, *et al.*, Two-Dimensional Nitrogen-Doped Ti_3C_2 Promoted Catalysis Performance of Silver Nanozyme for Ultrasensitive Detection of Hydrogen Peroxide, *ChemElectroChem*, 2022, **9**(10), e202200050.
22 R. Khan and S. Andreescu, MXenes-based bioanalytical sensors: Design, characterization, and applications, *Sensors*, 2020, **20**(18), 5434.
23 M. Huang, *et al.*, MXene and black phosphorus based 2D nanomaterials in bioimaging and biosensing: Progress and perspectives, *J. Mater. Chem. B*, 2021, **9**(26), 5195–5220.
24 J. Huang, *et al.*, Progress and biomedical applications of MXenes, *Nano Sel.*, 2021, **2**(8), 1480–1508.
25 Y. Xu, *et al.*, 2D-ultrathin MXene/DOXjade platform for iron chelation chemo-photothermal therapy, *Bioact. Mater.*, 2022, **14**, 76–85.

26 Y. Wang, *et al.*, MXenes: Focus on optical and electronic properties and corresponding applications, *Nanophotonics*, 2020, **9**(7), 1601–1620.
27 S. Li, *et al.*, New opportunities for emerging 2D materials in bioelectronics and biosensors, *Curr. Opin. Biomed. Eng.*, 2020, **13**, 32–41.
28 G. Liu, *et al.*, Surface modified Ti_3C_2 MXene nanosheets for tumor targeting photothermal/photodynamic/chemo synergistic therapy, *ACS Appl. Mater. Interfaces*, 2017, **9**(46), 40077–40086.
29 L. Bai, *et al.*, Surface modification engineering of two-dimensional titanium carbide for efficient synergistic multitherapy of breast cancer, *J. Mater. Chem. B*, 2020, **8**(30), 6402–6417.
30 A. Sundaram, *et al.*, Engineering of 2D transition metal carbides and nitrides MXenes for cancer therapeutics and diagnostics, *J. Mater. Chem. B*, 2020, **8**(23), 4990–5013.
31 A. Sundaram, *et al.*, *Transition metal carbide—MXene*, in *Handbook of Carbon-Based Nanomaterials*, Elsevier, 2021, pp. 671–709.
32 A. B. Sengul and E. Asmatulu, Toxicity of metal and metal oxide nanoparticles: a review, *Environ. Chem. Lett.*, 2020, **18**(5), 1659–1683.
33 M. S. Chavali and M. P. Nikolova, Metal oxide nanoparticles and their applications in nanotechnology, *SN Appl. Sci.*, 2019, **1**(6), 1–30.
34 K. ur Rehman, *et al.*, A Coronopus didymus based eco-benign synthesis of Titanium dioxide nanoparticles (TiO_2 NPs) with enhanced photocatalytic and biomedical applications, *Inorg. Chem. Commun.*, 2022, **137**, 109179.
35 J. Jiang, J. Pi and J. Cai, The advancing of zinc oxide nanoparticles for biomedical applications, *Bioinorg. Chem. Appl.*, 2018, **2018**, 1062562.
36 T. V. Tran, *et al.*, Green synthesis of ZrO_2 nanoparticles and nanocomposites for biomedical and environmental applications: a review, *Environ. Chem. Lett.*, 2022, 1–23.
37 M. Mahdavi, *et al.*, Synthesis, surface modification and characterisation of biocompatible magnetic iron oxide nanoparticles for biomedical applications, *Molecules*, 2013, **18**(7), 7533–7548.
38 M. Wu, *et al.*, Manganese dioxide nanosheets: from preparation to biomedical applications, *Int. J. Nanomed.*, 2019, **14**, 4781.
39 F. L. Rashid, *et al.*, Novel phase change materials, MgO nanoparticles, and water based nanofluids for thermal energy storage and biomedical applications, *Int. J. Pharm. Phytopharm. Res.*, 2018, **8**(1), 46–56.
40 A. B. Shcherbakov, *et al.*, CeO_2 nanoparticle-containing polymers for biomedical applications: A review, *Polymers*, 2021, **13**(6), 924.
41 M. E. Grigore, *et al.*, Methods of synthesis, properties and biomedical applications of CuO nanoparticles, *Pharmaceuticals*, 2016, **9**(4), 75.
42 A. Maleki, *et al.*, Biomedical Applications of MXene-Integrated Composites: Regenerative Medicine, Infection Therapy, Cancer Treatment, and Biosensing, *Adv. Funct. Mater.*, 2022, **32**(34), 2203430.
43 P. Iravani, S. Iravani and R. S. Varma, MXene-chitosan composites and their biomedical potentials, *Micromachines*, 2022, **13**(9), 1383.
44 L. Chen, *et al.*, Biomedical Applications of MXenes: From Nanomedicine to Biomaterials, *Acc. Mater. Res.*, 2022, **3**(8), 785–798.
45 A.-Z. Warsi, *et al.*, Synthesis, Characterization, Photocatalysis, and Anti-bacterial Study of WO_3, MXene and WO_3/MXene Nanocomposite, *Nanomaterials*, 2022, **12**(4), 713.
46 I. A. Alsafari, Synthesis of CuO/MXene nanocomposite to study its photocatalytic and anti-bacterial properties, *Ceram. Int.*, 2022, **48**(8), 10960–10968.
47 G. Liu, *et al.*, Magnetically separable MXene@ Fe_3O_4/Au/PDA nanosheets with photothermal-magnetolytic coupling anti-bacterial performance, *Appl. Surf. Sci.*, 2022, **590**, 153125.
48 M. Ding, *et al.*, Novel α-Fe_2O_3/MXene nanocomposite as heterogeneous activator of peroxymonosulfate for the degradation of salicylic acid, *J. Hazard. Mater.*, 2020, **382**, 121064.
49 K. Chaudhuri, *et al.*, *Optical properties of MXenes*, in *2D Metal Carbides and Nitrides (MXenes)*, Springer, 2019, pp. 327–346.
50 K. Hantanasirisakul, *et al.*, Fabrication of $Ti_3C_2T_x$ MXene transparent thin films with tunable optoelectronic properties, *Adv. Electron. Mater.*, 2016, **2**(6), 1600050.
51 X. Jiang, *et al.*, Broadband nonlinear photonics in few–layer MXene $Ti_3C_2T_x$ (T = F, O, or OH), *Laser Photonics Rev.*, 2018, **12**(2), 1700229.
52 B. Fu, *et al.*, MXenes: Synthesis, optical properties, and applications in ultrafast photonics, *Small*, 2021, **17**(11), 2006054.
53 B. Onel, *et al.*, A new G-quadruplex with hairpin loop immediately upstream of the human BCL2 P1 promoter modulates transcription, *J. Am. Chem. Soc.*, 2016, **138**(8), 2563–2570.
54 X. Jiang, *et al.*, Two-dimensional MXenes: From morphological to optical, electric, and magnetic properties and applications, *Phys. Rep.*, 2020, **848**, 1–58.
55 C. Wang, *et al.*, The SnO_2/MXene Composite Ethanol Sensor Based on MEMS Platform, *Chemosensors*, 2022, **10**(3), 109.
56 J. Low, *et al.*, TiO_2/MXene Ti_3C_2 composite with excellent photocatalytic CO_2 reduction activity, *J. Catal.*, 2018, **361**, 255–266.
57 Y. Zhu, *et al.*, MnO_2-MXene Composite as Electrode for Supercapacitor, *J. Electrochem. Soc.*, 2022, **169**(3), 030524.
58 T. Rasheed, *et al.*, A cost-effective approach to synthesize $NiFe_2O_4$/MXene heterostructures for enhanced photodegradation performance and anti-bacterial activity, *Adv. Powder Technol.*, 2021, **32**(7), 2248–2257.
59 A. Iqbal, *et al.*, Improving oxidation stability of 2D MXenes: synthesis, storage media, and conditions, *Nano Convergence*, 2021, **8**(1), 1–22.

60 X. Zhao, M. Radovic and M. J. Green, Synthesizing MXene nanosheets by water-free etching, *Chem*, 2020, **6**(3), 544–546.
61 N. Akhtar, *et al.*, Synthesis and characterization of MXene/$BiCr_2O_4$ nanocomposite with excellent electrochemical properties, *J. Mater. Res. Technol.*, 2021, **15**, 2007–2015.
62 N. Ottman, *et al.*, Soil exposure modifies the gut microbiota and supports immune tolerance in a mouse model, *J. Allergy Clin. Immunol.*, 2019, **143**(3), 1198–1206.
63 C. Liu, *et al.*, Synthesis of MXene/COF/Cu_2O heterojunction for photocatalytic bactericidal activity and mechanism evaluation, *Chem. Eng. J.*, 2022, **430**, 132663.
64 W. Wang, *et al.*, A photo catalyst of cuprous oxide anchored MXene nanosheet for dramatic enhancement of synergistic anti-bacterial ability, *Chem. Eng. J.*, 2020, **386**, 124116.
65 M. Z. Jakubczak, *Evaluation of the effectiveness of anti-bacterial filtration materials modified with nanocomponents based on Ti_3C_2*, Zakład Biologii, 2020.
66 X. Lian, *et al.*, Electrical Properties and Biological Synaptic Simulation of Ag/MXene/SiO_2/Pt RRAM Devices, *Electronics*, 2020, **9**(12), 2098.
67 K. S. Ranjith, *et al.*, An ultrasensitive electrochemical sensing platform for rapid detection of rutin with a hybridized 2D–1D MXene-$FeWO_4$ nanocomposite, *Sens. Actuators, B*, 2021, **344**, 130202.
68 M. Malaki, A. Maleki and R. S. Varma, MXenes and ultrasonication, *J. Mater. Chem. A*, 2019, **7**(18), 10843–10857.
69 I. A. Alsafari, *et al.*, Synthesis, characterization, photocatalytic and anti-bacterial properties of copper Ferrite/MXene ($CuFe_2O_4/Ti_3C_2$) nanohybrids, *Ceram. Int.*, 2021, **47**(20), 28874–28883.
70 H. B. Na, *et al.*, Development of a T_1 contrast agent for magnetic resonance imaging using MnO nanoparticles, *Angew. Chem.*, 2007, **119**(28), 5493–5497.
71 K. Rasool, *et al.*, Anti-bacterial activity of $Ti_3C_2T_x$ MXene, *ACS Nano*, 2016, **10**(3), 3674–3684.
72 L. Liu, *et al.*, A reactive copper-organophosphate-MXene heterostructure enabled anti-bacterial, self-extinguishing and mechanically robust polymer nanocomposites, *Chem. Eng. J.*, 2022, **430**, 132712.
73 S. Begum, *et al.*, 2D and heterostructure nanomaterial based strategies for combating drug-resistant bacteria, *ACS Omega*, 2020, **5**(7), 3116–3130.
74 H. Zheng, *et al.*, Bioactive anti-inflammatory, anti-bacterial, conductive multifunctional scaffold based on MXene@ CeO_2 nanocomposites for infection-impaired skin multimodal therapy, *Chem. Eng. J.*, 2021, **424**, 130148.
75 A. Rozmysłowska-Wojciechowska, *et al.*, Influence of modification of Ti_3C_2 MXene with ceramic oxide and noble metal nanoparticles on its antimicrobial properties and ecotoxicity towards selected algae and higher plants, *RSC Adv.*, 2019, **9**(8), 4092–4105.
76 T. Tahir, *et al.*, Synthesis of sponge like Gd^{3+} doped vanadium oxide/2D MXene composites for improved degradation of industrial effluents and pathogens, *Ceram. Int.*, 2022, **48**(2), 1969–1980.
77 K. Rajavel, *et al.*, Photocatalytic and bactericidal properties of MXene-derived graphitic carbon-supported TiO_2 nanoparticles, *Appl. Surf. Sci.*, 2021, **538**, 148083.
78 S. Tohme, R. L. Simmons and A. Tsung, Surgery for cancer: a trigger for metastases, *Cancer Res.*, 2017, **77**(7), 1548–1552.
79 Y. S. Birhan and H.-C. Tsai, Recent developments in selenium-containing polymeric micelles: prospective stimuli, drug-release behaviors, and intrinsic anticancer activity, *J. Mater. Chem. B*, 2021, **9**(34), 6770–6801.
80 R. Baskar, *et al.*, Cancer and radiation therapy: current advances and future directions, *Int. J. Med. Sci.*, 2012, **9**(3), 193.
81 I. dos Santos Guimarães, *et al.*, *Conventional cancer treatment, in Cancer Treatment-Conventional and Innovative Approaches*, IntechOpen, 2013.
82 T. A. Baudino, Targeted cancer therapy: the next generation of cancer treatment, *Curr. Drug Discovery Technol.*, 2015, **12**(1), 3–20.
83 A. Sundaram, *et al.*, Advanced nanomaterials for hypoxia tumor therapy: challenges and solutions, *Nanoscale*, 2020, **12**(42), 21497–21518.
84 X. Han, *et al.*, 2D ultrathin MXene–based drug–delivery nanoplatform for synergistic photothermal ablation and chemotherapy of cancer, *Adv. Healthcare Mater.*, 2018, **7**(9), 1701394.
85 L. M. Dong, *et al.*, Two-dimensional metal carbides and nitrides (MXenes): preparation, property, and applications in cancer therapy, *Nanophotonics*, 2020, **9**(8), 2125–2145.
86 A. Gazzi, *et al.*, Photodynamic therapy based on graphene and MXene in cancer theranostics, *Front. Bioeng. Biotechnol.*, 2019, **7**, 295.
87 M. Abbas, *et al.*, *Nanotechnology for cancer drug design, delivery, and theranostics applications*, in *Biogenic Nanoparticles for Cancer Theranostics*, Elsevier, 2021, pp. 1–26.
88 Z. Huang, *et al.*, Two-dimensional MXene-based materials for photothermal therapy, *Nanophotonics*, 2020, **9**(8), 2233–2249.
89 S. Shurbaji, *et al.*, Characterization of MXene as a cancer photothermal agent under physiological conditions, *Front. Nanotechnol.*, 2021, 63.
90 C. Dai, H. Lin, G. Xu, Z. Liu, R. Wu and Y. Chen, Biocompatible 2D titanium carbide (MXenes) composite nanosheets for pH-responsive MRI-guided tumor hyperthermia, *Chem. Mater.*, 2017, **29**(20), 8637–8652.
91 Z. Liu, *et al.*, 2D superparamagnetic tantalum carbide composite MXenes for efficient breast-cancer theranostics, *Theranostics*, 2018, **8**(6), 1648.
92 H. Xiang, *et al.*, Hypoxia-irrelevant photonic thermodynamic cancer nanomedicine, *ACS Nano*, 2019, **13**(2), 2223–2235.
93 D.-Y. Zhang, *et al.*, *In situ* TiO_{2-x} decoration of titanium carbide MXene for photo/sono-responsive antitumor theranostics, *J. Nanobiotechnol.*, 2022, **20**(1), 1–14.

94 Z. Liu, *et al.*, Redox chemistry-enabled stepwise surface dual nanoparticle engineering of 2D MXenes for tumor-sensitive T_1 and T_2 MRI-guided photonic breast-cancer hyperthermia in the NIR-II biowindow, *Biomater. Sci.*, 2022, **10**(6), 1562–1574.
95 X. Zhang, *et al.*, Ti_3C_2-MXene@N-doped carbon heterostructure-based electrochemical sensor for simultaneous detection of heavy metals, *J. Electroanal. Chem.*, 2022, **911**, 116239.
96 D. Yi, *et al.*, Ti_3CN MXene-based ultra-sensitive optical fiber salinity sensor, *Opt. Lett.*, 2022, **47**(1), 138–141.
97 Y. Pei, *et al.*, $Ti_3C_2T_X$ MXene for sensing applications: recent progress, design principles, and future perspectives, *ACS Nano*, 2021, **15**(3), 3996–4017.
98 M. Xin, *et al.*, MXenes and their applications in wearable sensors, *Front. Chem.*, 2020, **8**, 297.
99 K. Grabowski, *et al.*, Recent advances in MXene-based sensors for Structural Health Monitoring applications: a review, *Measurement*, 2021, 110575.
100 B. Xu, C. Zhi and P. Shi, Latest advances in MXene biosensors, *J. Phys.: Mater.*, 2020, **3**(3), 031001.
101 A. Sinha, *et al.*, *MXene-based sensors and biosensors: next-generation detection platforms*, in *Handbook of Nanomaterials in Analytical Chemistry*, Elsevier, 2020, pp. 361–372.
102 R. Thenmozhi, *et al.*, MXene Based Transducer for Biosensor Applications, *J. Electrochem. Soc.*, 2021, **168**, 117507.
103 C. Verma and K. K. Thakur, Recent advances in MXene-based electrochemical sensors, *Eur. J. Mol. Clin. Med.*, 2020, **7**, 4429–4450.
104 D. Guo, G. Xie and J. Luo, Mechanical properties of nanoparticles: basics and applications, *J. Phys. D: Appl. Phys.*, 2013, **47**(1), 013001.
105 T. Sebastian and F. Clemens, Piezoelectric application of metal oxide nanofibers, in *Metal Oxide-Based Nanofibers and Their Applications*, Elsevier, 2022, pp. 215–246.
106 R. Parra and H. Farrell, Binding energy of metal oxide nanoparticles, *J. Phys. Chem. C*, 2009, **113**(12), 4786–4791.
107 M. A. Carpenter, S. Mathur and A. Kolmakov, *Metal oxide nanomaterials for chemical sensors*, Springer Science & Business Media, 2012.
108 R. A. Soomro, *et al.*, $NiWO_4$-induced partial oxidation of MXene for photo-electrochemical detection of prostate-specific antigen, *Sens. Actuators, B*, 2021, **328**, 129074.
109 G. Chen, *et al.*, Efficient Z-Scheme heterostructure based on $TiO_2/Ti_3C_2T_x/Cu_2O$ to boost photoelectrochemical response for ultrasensitive biosensing, *Sens. Actuators, B*, 2020, **312**, 127951.
110 S. Boobphahom, *et al.*, TiO_2/MXene-PVA/GO hydrogel-based electrochemical sensor for neurological disorder screening via urinary norepinephrine detection, *Microchim. Acta*, 2021, **188**(11), 1–12.
111 F. Wang, *et al.*, TiO_2 nanoparticle modified organ-like Ti_3C_2 MXene nanocomposite encapsulating hemoglobin for a mediator-free biosensor with excellent performances, *Biosens. Bioelectron.*, 2015, **74**, 1022–1028.
112 X. Lu, *et al.*, A covalent organic polymer–TiO_2/Ti_3C_2 heterostructure as nonenzymatic biosensor for voltammetric detection of dopamine and uric acid, *Microchim. Acta*, 2021, **188**(3), 1–11.
113 C. He, *et al.*, Combinatorial Photothermal 3D-Printing Scaffold and Checkpoint Blockade Inhibits Growth/Metastasis of Breast Cancer to Bone and Accelerates Osteogenesis, *Adv. Funct. Mater.*, 2021, **31**(10), 2006214.
114 J. K. Wychowaniec, *et al.*, Unique cellular network formation guided by heterostructures based on reduced graphene oxide - $Ti_3C_2T_x$ MXene hydrogels, *Acta Biomater.*, 2020, **115**, 104–115.
115 B. Guo and P. X. Ma, Conducting Polymers for Tissue Engineering, *Biomacromolecules*, 2018, **19**(6), 1764–1782.
116 K. Dzobo, *et al.*, Advances in Regenerative Medicine and Tissue Engineering: Innovation and Transformation of Medicine, *Stem Cells Int.*, 2018, **2018**, 2495848.
117 M. Tang, *et al.*, Dual active nanozyme-loaded MXene enables hyperthermia-enhanced tumor nanocatalytic therapy, *Chem. Eng. J.*, 2022, **449**, 137847.
118 H. Lin, *et al.*, Two-Dimensional Ultrathin MXene Ceramic Nanosheets for Photothermal Conversion, *Nano Lett.*, 2017, **17**(1), 384–391.
119 H. Lin, Y. Chen and J. Shi, Insights into 2D MXenes for Versatile Biomedical Applications: Current Advances and Challenges Ahead, *Adv. Sci.*, 2018, **5**(10), 1800518.
120 H. Lin, *et al.*, A Two-Dimensional Biodegradable Niobium Carbide (MXene) for Photothermal Tumor Eradication in NIR-I and NIR-II Biowindows, *J. Am. Chem. Soc.*, 2017, **139**(45), 16235–16247.
121 W. Feng, *et al.*, Ultrathin Molybdenum Carbide MXene with Fast Biodegradability for Highly Efficient Theory-Oriented Photonic Tumor Hyperthermia, *Adv. Funct. Mater.*, 2019, **29**(22), 1901942.
122 H. Cao, *et al.*, A Genetic Algorithm Based Motor Controller System Automatic Layout Method, in *2019 10th International Conference on Power Electronics and ECCE Asia (ICPE 2019 - ECCE Asia)*, 2019.
123 Z. Xie, *et al.*, Biocompatible Two-Dimensional Titanium Nanosheets for Multimodal Imaging-Guided Cancer Theranostics, *ACS Appl. Mater. Interfaces*, 2019, **11**(25), 22129–22140.
124 C. Dai, *et al.*, Two-dimensional tantalum carbide (MXenes) composite nanosheets for multiple imaging-guided photothermal tumor ablation, *ACS Nano*, 2017, **11**(12), 12696–12712.
125 Y. Sun, *et al.*, In situ growth of TiO_2 nanowires on Ti_3C_2 MXenes nanosheets as highly sensitive luminol electrochemiluminescent nanoplatform for glucose detection in fruits, sweat and serum samples, *Biosens. Bioelectron.*, 2021, **194**, 113600.
126 J. Csavina, *et al.*, Effect of wind speed and relative humidity on atmospheric dust concentrations in semi-arid climates, *Sci. Total Environ.*, 2014, **487**, 82–90.

127 V. Myndrul, *et al.*, MXene nanoflakes decorating ZnO tetrapods for enhanced performance of skin-attachable stretchable enzymatic electrochemical glucose sensor, *Biosens. Bioelectron.*, 2022, **207**, 114141.
128 M. P. Browne, D. Tyndall and V. Nicolosi, *Curr. Opin. Electrochem.*, 2022, **34**, 101021.
129 L. Tan, J. Lv, X. Xu, H. Zhao, C. He, H. Wang and W. Zheng, *Ceram. Int.*, 2019, **45**, 6597–6600.
130 G. Murali, J. K. Reddy Modigunta, Y. H. Park, J. H. Lee, J. Rawal, S. Y. Lee, I. In and S. J. Park, *ACS Nano*, 2022, **16**, 13370–13429.
131 R. B. Rakhi, B. Ahmed, D. H. Anjum and H. N. Alshareef, *ACS Appl. Mater. Interfaces*, 2016, **8**, 18806–18814.
132 W. Xi, J. Jin, Y. Zhang, R. Wang, Y. Gong, B. He and H. Wang, *Nanoscale*, 2022, **14**, 11923–11944.
133 C. Li, G. Jiang, M. Demir, Y. Sun, R. Wang and T. Liu, *J. Energy Storage*, 2022, **56**, 105986.